JOURNAL OF MATERIALS SCIENCE 28 (1993) 1585–1594

# Low-stress creep behaviour of superplastic Zn–22% Al alloy

N. PRASAD
*Department of Metallurgical Engineering, Banaras Hindu University, Varanasi 221 005, India*
G. MALAKONDAIAH, D. BANERJEE
*Defence Metallurgical Research Laboratory, Hyderabad 500 258, India*
P. RAMA RAO
*Department of Science and Technology, Government of India, New Delhi 110 016, India*

Low-stress creep behaviour of microduplex Zn–22% Al alloy was studied using spring specimen geometry. The average phase size in the specimens investigated was 0.87, 1.48 and 1.98 μm. Experiments were conducted in the temperature range 393–473 K at stresses below about 1.0 MN m$^{-2}$. The present study has established that the stress exponent of the creep rate is unity and, therefore, a viscous creep process dominates the flow in Region I superplasticity. The activation energy corresponds to that for boundary diffusion. However, the phase-size exponent was found to be −2 instead of −3, as predicted by the Coble creep theory. Further, the measured creep rates are three to four orders of magnitude slower than those predicted by the Coble theory. Transmission electron microscopy revealed precipitation, along α/α grain interfaces, whose inhibiting action on plastic flow should at least be partly responsible for the lower values of measured creep rates. There also exist two other interfaces, namely α/β and β/β, whose comprehensive role in diffusion creep is not yet fully understood. Therefore, it seems illogical to describe the creep behaviour of Zn–22% Al by the classical Coble theory, originally developed for single-phase polycrystals.

## 1. Introduction

Superplastic materials usually exhibit a sigmoidal relationship between stress, σ, and strain rate, $\dot{\varepsilon}$, with three distinct regions, designated I, II and III, at low, intermediate and high strain rates, respectively (Fig. 1). Regions I and III are characterized by a low strain-rate sensitivity ($m \sim 0.25$), whereas in Region II, $m$ attains a higher value of 0.5 or more. Region II, where the material exhibits superplasticity, has been widely studied and the flow characteristics are well understood. At higher strain rates a transition occurs from Region II to Region III and the change in the behaviour is documented reasonably well. On the other hand, at lower strain rates, in Region I, the behaviour is not so clear, even though this has been the subject of numerous investigations [1].

From the point of view of Region I behaviour, Zn–Al alloys, among the superplastic alloys, have been examined somewhat more widely. In these alloys two separate trends have been reported in the literature. Early experiments on Zn–22% Al by Vaidya *et al.* [2] have shown that the value of stress exponent of strain rate, $n$, in Region I, was low (about 1) and these authors suggested diffusion creep to be the flow mechanism. This trend has been subsequently confirmed by Mukherjee and co-workers [3, 4]. Recent experiments by Mishra and Murty [5] also showed the existence of Region I with strain-rate sensitivity ($m = 1/n$) approaching unity. In contrast, Langdon and co-workers [6–11], Grivas [12], Vale *et al.* [13], Livesey and Ridley [14] and recently Chaudhury and Mohamed [15] have reported, on the basis of their studies on Zn–22% Al and Pb–62% Sn alloys, a higher value of about 3–4 in Region I.

To resolve this discrepancy in the observed flow behaviour at low strain rates, detailed investigations have been undertaken by us on the Zn–22% Al alloy by employing an experimental technique capable of higher sensitivity. Close-coiled spring specimens, similar to those used for diffusion creep studies, have been

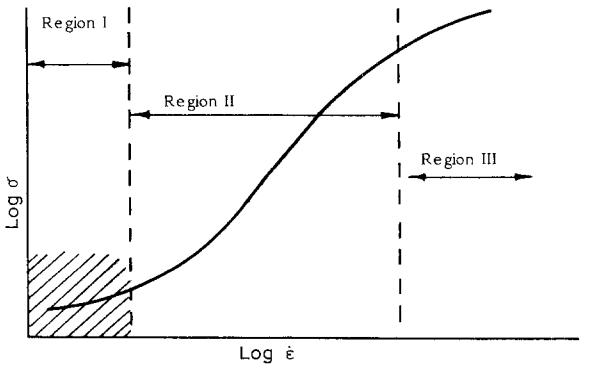


*Figure 1* The relationship between stress and strain rate for superplastic materials (schematic). Of interest in the present investigation is the cross-hatched Region I.

employed to record the Region I strain rates accurately. As emphasized earlier [16, 17] these specimens have several advantages when compared to conventional creep specimens. Because of their higher sensitivity, tests need not be continued, even to record low strain rates, for longer durations like in the conventional creep tests. Hence structural changes occurring during the testing period can be avoided. Further, because the specimens are self-loaded, testing one specimen will be equal to conducting a number of conventional creep tests as each coil of the specimen is subjected to a different stress depending on the number of coils below it.

## 2. Experimental procedure

The experimental alloy contained 20.9 wt % Al and the other elements as follows: (p.p.m.) 4000 Cu, 280 Fe, 100 Pb, 26 Mg, 20 Ni, 20 Cd and 10 Mn. Strips of 2.5 mm × 2.5 mm × 300 mm cut from the rolled sheet were wire drawn to a final diameter of 1.0 mm. Wires were then wound on a stainless steel mandrel and subjected to solution treatment, while on the mandrel, in an argon atmosphere at 633 K for 17 h before quenching in water. Subsequently, these mandrels, along with spring specimens, were annealed at 528 K for 1/3, 6 and 40 h to vary the phase size. Spring specimens were then unscrewed from the mandrel. Spring radius was maintained at 7.4 mm and the number of coils varied up to 10.

Scanning electron micrographs of the polished and etched surfaces were used to measure the intercept phase size, $\bar{L}$. More than 300 intercepts were considered in each case. Mean linear-intercept phase-size values were then converted to phase diameter, $d$, using the expression [18] $d = 1.776\,\bar{L}$. Treatments employed and the resulting phase sizes (referring to phase diameter) are given in Table I. The corresponding scanning electron micrographs are shown in Fig. 2.

Each spring specimen was allowed to creep under its own weight by suspending it from the top of a specially designed split furnace. The furnace was provided with a glass window to enable measurement of deflection of each coil. Coil deflections were monitored as a function of time with the help of a vertical cathetometer, located outside the furnace, focused on to the specimen with an accuracy of $\pm$ 10 μm. The furnace temperature was monitored through a mercury thermometer placed in close proximity to the specimen. The temperature variation was maintained within $\pm$ 1.5 K using a proportional temperature controller.

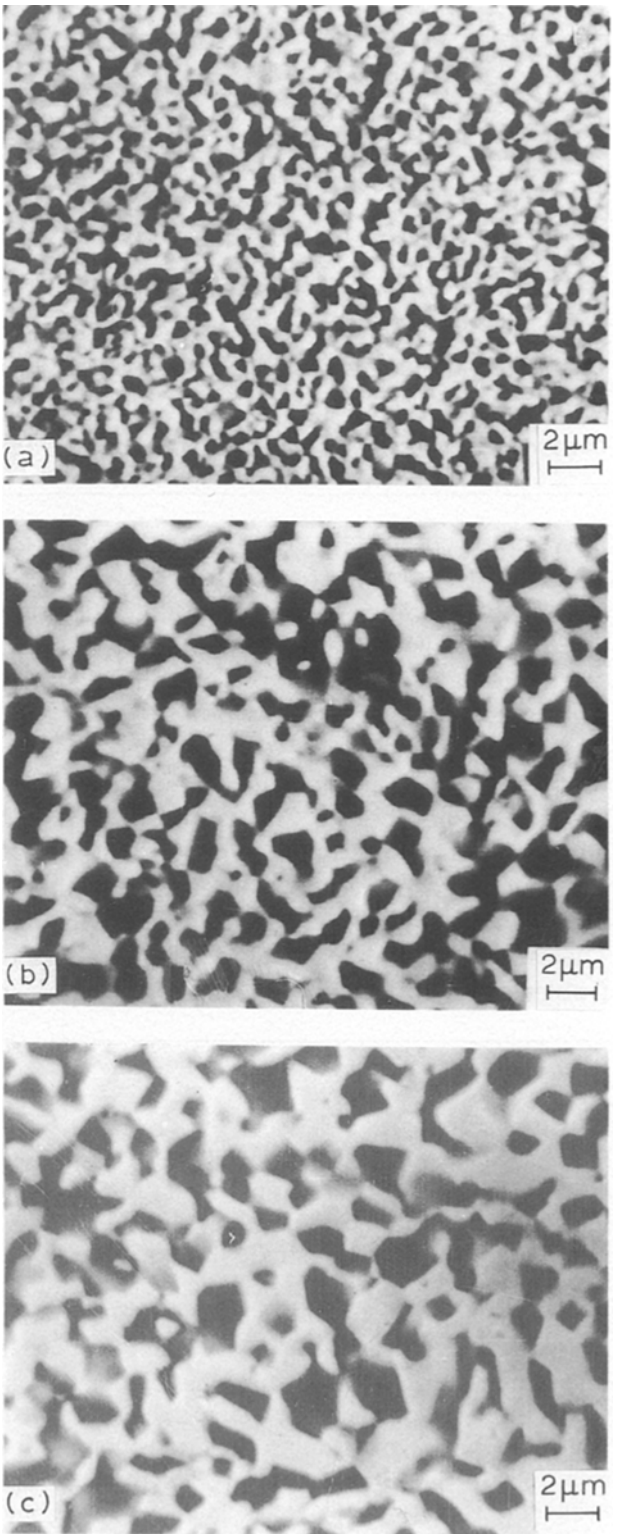


*Figure 2* Scanning electron micrographs of Zn–22% Al alloy aged at 523 K for (a) 1/3 h, (b) 6 h and (c) 40 h.

TABLE I Thermal treatments developed to vary phase size in Zn–22% Al alloy

| Serial no. | Treatment[a] | Average phase size, $d$ (μm) |
|---|---|---|
| 1 | 633 K/17 h (Ar), WQ + 523 K/1/3 h | 0.87 |
| 2 | 633 K/17 h (Ar), WQ + 523 K/6 h | 1.48 |
| 3 | 633 K/17 h (Ar), WQ + 523 K/40 h | 1.98 |

[a] Ar, argon atmosphere; WQ, water quenched.

Phase-size measurement carried out before and after the test revealed no detectable phase growth during the course of testing. After creep testing, in each case, spring dimensions and the weight of each coil were determined. Coil deflection rates and the load acting upon each coil were converted to creep rates, $\dot{\varepsilon}$, and stresses, $\sigma$, respectively, using the expressions given elsewhere [16, 17].

Foils for transmission electron microscopy were prepared by grinding the wire specimens (from which the spring specimens for creep tests were made) along their length so that flat specimens of width about 1.0 mm were obtained. These were lacquered along the edges to prevent excessive edge attack during polishing and immersed in an agitated bath of 20% perchloric acid and 80% methanol at 253 K at a potential of 17 V. After perforation occurred, the wire was removed and a scalpel used to cut off specimens from the edges of the perforation. Some preferential attack of the aluminium-rich phase could not be prevented. The thin foils were examined in a Philips 430 T electron microscope equipped with an EDAX analyser.

## 3. Results and discussion

Low-stress creep experiments were conducted on specimens with phase size 0.87, 1.48 and 1.98 μm over the range of temperature 393–473 K and stresses up to about 1.0 MN m$^{-2}$. The experimental conditions employed are given in Table II.

Prior to the onset of steady-state creep, there exists in all cases a transient stage during which deflection rate decreases with time. Deflection versus time curves shown in Fig. 3 clearly indicate this feature. It is also evident from Fig. 3 that the transient strain (deflection is proportional to strain) increases with increasing stress. Steady-state creep rates derived from the slopes of deflection versus time curves in the steady-state region only are considered in the analysis presented here. Using spring specimen geometry it was possible to record accurately creep rates as low as $10^{-9}$ s$^{-1}$, which are more than an order of magnitude lower than the lowest reported values of around $10^{-8}$ s$^{-1}$, except in the case of Vale *et al.* [13]; Table III.

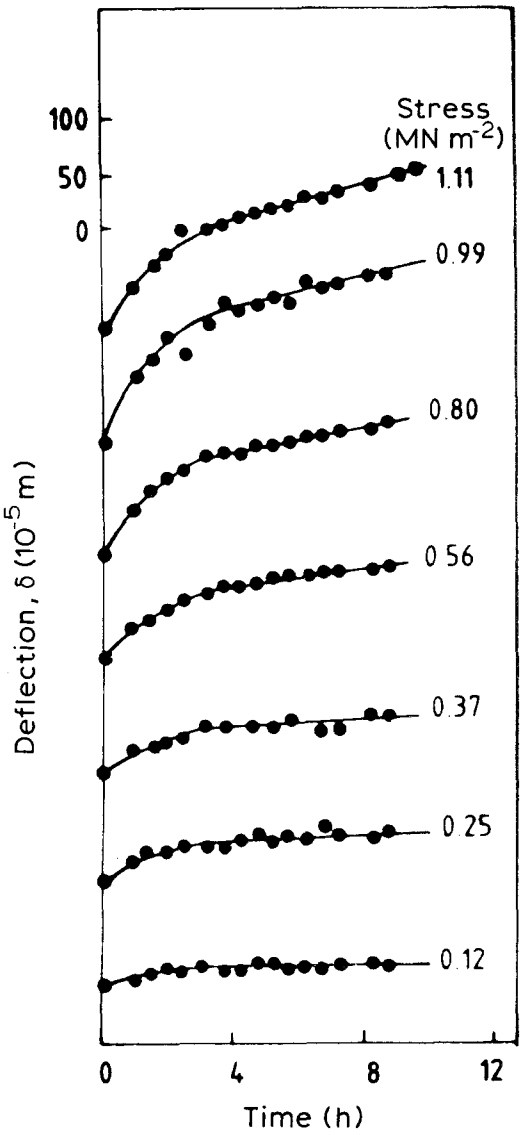


*Figure 3* Typical deflection–time curves for Zn–22% Al of phase size 1.98 μm obtained at 433 K.

TABLE II Experimental conditions employed

| Test no. | $d$ (μm) | Test temperature, $T$ (K) | Test duration (h) | Maximum applied stress, σ (MN m$^{-2}$) |
|---|---|---|---|---|
| SP-1 | 0.87 | 393 | 8.5 | 0.86 |
| SP-2 | 0.87 | 413 | 4.8 | 0.62 |
| SP-3 | 0.87 | 433 | 5.0 | 0.49 |
| SP-4 | 0.87 | 453 | 2.0 | 0.49 |
| SP-5 | 1.48 | 413 | 8.0 | 0.62 |
| SP-6 | 1.48 | 433 | 8.0 | 0.98 |
| SP-7 | 1.48 | 453 | 6.0 | 0.62 |
| SP-8 | 1.48 | 473 | 3.0 | 0.49 |
| SP-9 | 1.98 | 433 | 9.0 | 1.11 |
| SP-10 | 1.98 | 450 | 8.0 | 0.98 |
| SP-11 | 1.98 | 473 | 6.0 | 0.87 |

Strain rate is linearly proportional to stress in all cases. For tests where the stress range extended beyond about 0.8 MN m$^{-2}$, a deviation from linearity was observed at higher stresses. One such case is shown in Fig. 4. Beyond 0.8 MN m$^{-2}$, creep rate increases steeply with increase in stress, thus indicating a transition from one mechanism to another. This aspect will be commented upon further in a later

TABLE III Strain rate range studied and test conditions employed by various investigators

| Strain rate, $\dot{\varepsilon}$ (s$^{-1}$) | Grain size, $d$, (μm) | Test temp. (K) | Reference |
|---|---|---|---|
| $2.0\times10^{-8}$–$1.3\times10^{-1}$ | 1.19–4.62 | 448–523 | Vaidya *et al.* [2] |
| $1.0\times10^{-7}$–$1.5\times10^{-2}$ | 1.3–3.7 | 450–525 | Arieli *et al.* [3] |
| $3.2\times10^{-8}$–$3.0\times10^{-2}$ | 2.1–7.5 | 403–503 | Mohamed and Langdon [7] |
| $1.8\times10^{-9}$–$1.0\times10^{-4}$ | 1.2–5.1 | 413–458 | Vale *et al.* [13] |
| $6.0\times10^{-7}$–$8.0\times10^{-2}$ | 2.8–4.1 | 423–523 | Livesey and Ridley [14] |
| $2.0\times10^{-8}$–$6.0\times10^{-2}$ | 2.1–4.4 | 413–503 | Mishra and Murty [5] |
| $5.8\times10^{-8}$–$3.5\times10^{-2}$ | 2.5 | 430–500 | Chaudhury and Mohamed [15] |
| $1.0\times10^{-9}$–$1.0\times10^{-7}$ | 0.87–1.98 | 393–473 | Present work |

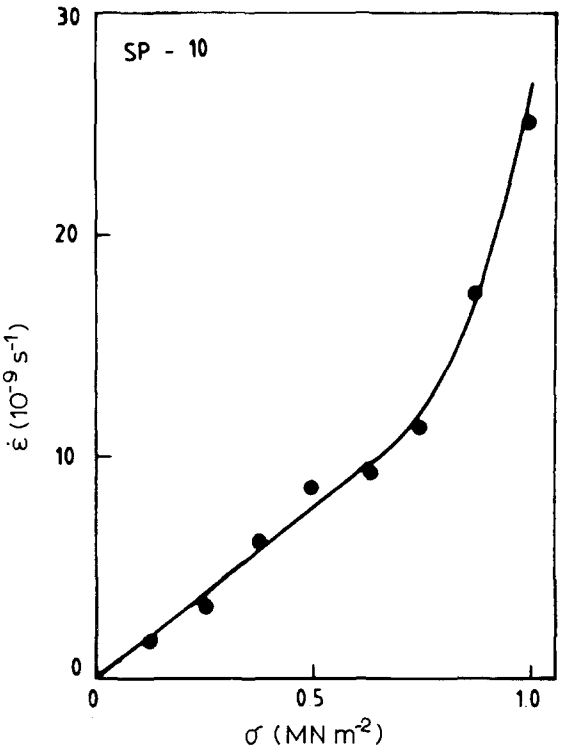


*Figure 4* A typical strain rate versus stress plot for Zn–22% Al of phase size 1.98 μm at 450 K.

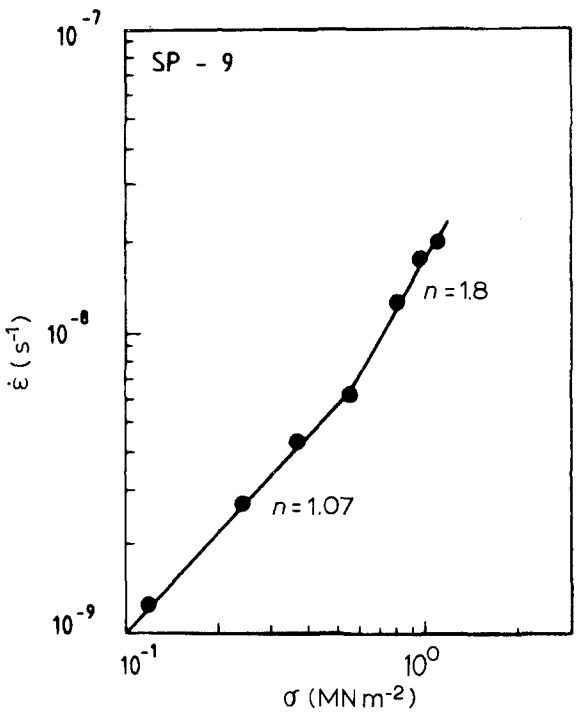


*Figure 5* A typical log–log plot of strain rate versus stress for Zn–22% Al of phase size 1.98 μm at 433 K.

section. The linear portion of the creep rate versus stress plot when extrapolated to zero strain rate nearly passes through the origin in all cases, indicating the absence of a threshold stress. This observation is contradictory to the behaviour reported recently by Chaudhury and Mohamed [15]. In a detailed study of the effect of impurities on the superplastic flow in Zn–22% Al alloy, Chaudhury and Mohamed [15] observed that the deformation characteristics are governed by the purity of the alloy. Significant threshold stress has been observed with two grades of the alloy containing 180 and 100 p.p.m. total impurities while the high-purity one with 6 p.p.m. impurity content showed no evidence of the threshold stress. Contrary to these observations, no evidence of threshold stress has been found in the present case despite the experimental material being a commercial alloy with a relatively large impurity content.

### 3.1. Strain-rate dependence on stress

Log $\dot{\varepsilon}$ versus log $\sigma$ plots in all cases have yielded a stress exponent of unity at stresses below about 0.8 MN $m^{-2}$. At stresses above the transition stress, the slope increases and approaches a value close to 2 (Fig. 5). A stress exponent of nearly 2 at stresses above about 0.8 MN $m^{-2}$ indicates Region II superplastic flow. Further, the value of the transition stress is in good agreement with the earlier reports on Zn–22% Al [2–4]. Because our main interest is to re-examine the Region I, creep data below the transition stress are analysed in detail in the following sections.

### 3.2. Strain-rate dependence on phase size

Strain rate per unit stress, $d\dot{\varepsilon}/d\sigma$, obtained at temperatures 413, 433, 453 and 473 K, is plotted against phase size on a log–log scale in Fig. 6. Although data are limited, these reveal an inverse square-phase size dependence of creep rate at these test temperatures.

### 3.3. Temperature dependence of strain rate

Logarithm of temperature-compensated creep rate per unit stress, $T\,d\dot{\varepsilon}/d\sigma$, is plotted against reciprocal of test temperature, $1/T$, in Fig. 7. The plots have yielded activation energies of 61.7, 61.6 and 62.9 kJ $mol^{-1}$ for

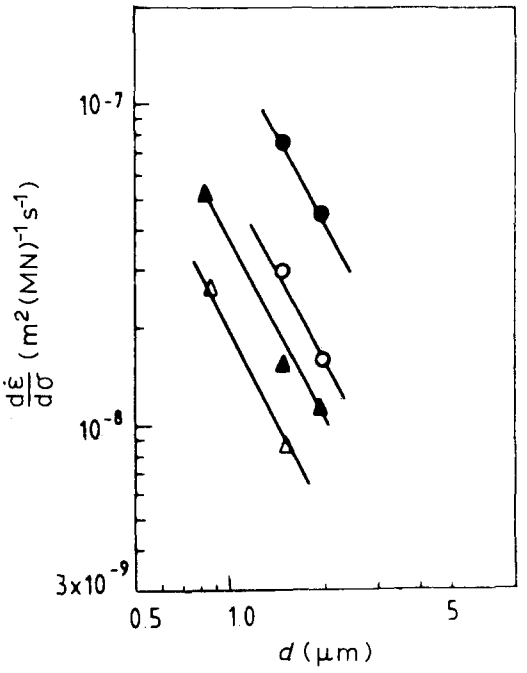


*Figure 6* Double logarithmic plot of strain rate per unit stress versus phase size at (△) 413, (▲) 433, (○) 453 and (●) 473 K for Zn–22% Al in the phase-size range 0.87–1.98 μm.

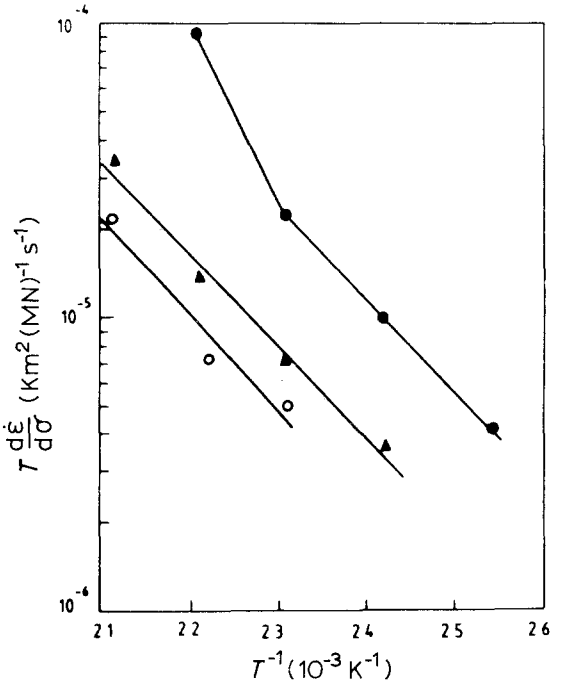


*Figure 7* Logarithm of temperature-compensated strain rate per unit stress plotted against reciprocal of absolute test temperature for Zn–22% Al in the phase-size range 0.87–1.98 μm. (●) 0.87 μm, $Q = 61.7\,kJ\,mol^{-1}$; (▲) 1.48 μm, $Q = 61.6\,kJ\,mol^{-1}$; (○) 1.98 μm, $Q = 62.9\,kJ\,mol^{-1}$.

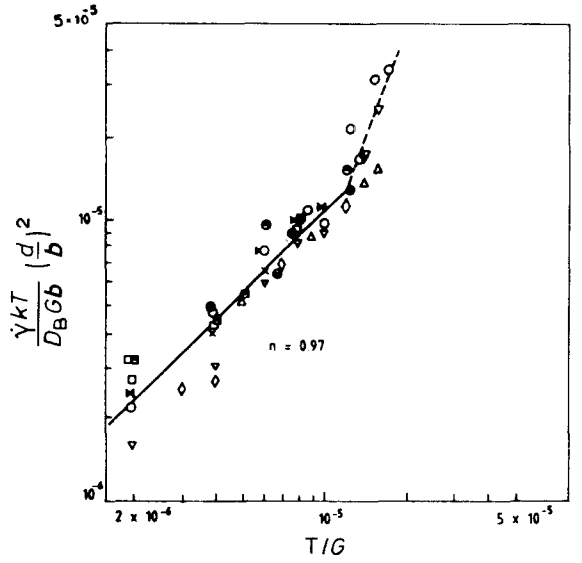


*Figure 8* Normalized shear strain rate versus normalized shear stress plot for Zn–22% Al over a phase size range 0.87–1.98 μm and in the temperature interval 393–473 K. *d*, *T*: (○) 0.87 μm, 393 K; (×) 0.87 μm, 413 K; (□) 0.87 μm, 433 K; (△) 1.48 μm, 433 K; (◇) 1.48 μm, 453 K; (⬓) 1.48 μm, 473 K; (⧓) 1.48 μm, 413 K; (○) 1.98 μm. 433 K; (▽) 1.98 μm, 450 K; (◓) 1.98 μm, 473 K.

the three phase sizes considered. The average of these measurements, $62\,kJ\,mol^{-1}$, matches well with the activation energy for grain-boundary self diffusion, $Q_B$, in zinc [19] ($59.9\,kJ\,mol^{-1}$) as compared to that for aluminium ($85.3\,kJ\,mol^{-1}$), estimated by taking $Q_B = 0.6\,Q_V$, where $Q_V$ is the lattice self-diffusion activation energy [20]. It should be noted that no such comparison is possible with interphase diffusion due to lack of data.

In the case of 0.87 μm phase size, Fig. 7 indicates a change in activation energy at temperatures above 433 K. The limited data do not permit estimation of reliable activation energy. However, joining the two data points yields an activation energy of $113.2\,kJ\,mol^{-1}$, which matches fairly well with that reported [21] for lattice self diffusion in pure zinc ($91.3\,kJ\,mol^{-1}$).

## 3.4. Experimental flow relationship

A flow relationship is derived by fitting the experimental data to the semi-empirical equation, applied extensively in experimental investigations of superplasticity [1, 22], namely

$$\dot{\gamma} = A(D_0Gb/kT)(b/d)^p(\tau/G)^n\exp(-Q/RT) \quad (1)$$

where $A$ is a dimensionless constant, $\dot{\gamma}$ the shear strain rate, $\tau$ the shear stress, $G$ the shear modulus, $b$ the Burgers vector, $d$ the average phase size, $R$ the gas constant and $kT$ has the usual meaning. $D_0$ and $Q$ are the frequency factor and activation energy associated with the appropriate diffusion coefficient. $p$ and $n$ are normalized grain size and stress exponents, respectively.

The analysis presented in the preceeding sections has resulted in $p = 2$ and $Q = 62\,kJ\,mol^{-1}$. To determine $A$ and $n$, creep data obtained in the present study are presented in Fig. 8 as normalized creep rate $[(\dot{\gamma}kT/D_BGb)(b/d)^2$, where $D_B$ is boundary diffusivity] versus normalized stress ($\tau/G$). Shear modulus at a given temperature is estimated using the expression [8] $G_{alloy} = 4.797\times10^4 - 26.62\,T$, where $G$ and $T$ are expressed in $MN\,m^{-2}$ and Kelvin, respectively. The frequency factor $D_{0_B}$ and $b$ are assumed to be $10^{-4}\,m^2\,s^{-1}$ and $2.7\times10^{-10}$ m, respectively. A least-squares fit to the data points shown in Fig. 8 yields a slope of 1 for Region I. Measured creep rates in Region I superplasticity can thus be represented by the relationship

$$\dot{\gamma} = 8\times10^{-6}\frac{D_{0_B}G\,b}{kT}\left(\frac{b}{d}\right)^2\left(\frac{\tau}{G}\right)^{1.0}\exp\left(\frac{-62\,000}{RT}\right) \quad (2)$$

A stress exponent of unity and a strong phase-size dependence indicate relevance and dominance of a diffusion creep process in Region I. However, the experimental creep relationship given above does not match either of the two well-understood diffusion creep processes, namely Nabarro [23]–Herring [24] (N–H) and Coble [25]. Although the measured activation energy suggests Coble creep as the dominating flow process, phase-size dependence (exponent of $-2$) does not match the theoretical value (exponent of $-3$) for Coble creep. On the other hand, although phase-size dependence matches the N–H creep prediction, activation energies do not agree. The dimensionless constant has a very low value ($8\times10^{-6}$) and does not match either that of the Coble (143.2) or N–H (40) creep process.

TABLE IV Experimental relationships obtained for Zn–22% Al in Region I

| Reference | Relationship |
|---|---|
| Vaidya *et al.* [2] | $\dot{\gamma} = 0.17 \frac{D_0 G b}{kT} \left(\frac{b}{d}\right)^{2.5} \left(\frac{\tau}{G}\right)^{0.87} \exp\left(-\frac{74\,500}{RT}\right)$ |
| Misro and Mukherjee [4] | $\dot{\gamma} = 170 \frac{D_0 G b}{kT} \left(\frac{b}{d}\right)^{3.0} \left(\frac{\tau}{G}\right)^{1.0} \exp\left(-\frac{64\,500}{RT}\right)$ |
| Arieli *et al.* [3] | $\dot{\gamma} = 10 \frac{D_0 G b}{kT} \left(\frac{b}{d}\right)^{2.0} \left(\frac{\tau}{G}\right)^{1.0} \exp\left(-\frac{95\,900}{RT}\right)$ |
| Langdon and co-workers [7, 8] | $\dot{\gamma} = 2.5 \times 10^{17} \frac{D_0 G b}{kT} \left(\frac{b}{d}\right)^{2.4} \left(\frac{\tau}{G}\right)^{3.8} \exp\left(-\frac{119\,000}{RT}\right)$ |
| Vale *et al.* [13] | $\dot{\gamma} = 3.7 \times 10^{12} \frac{D_0 G b}{kT} \left(\frac{b}{d}\right)^{2.8} \left(\frac{\tau}{G}\right)^{3.1} \exp\left(-\frac{89\,000}{RT}\right)$ |
| Chaudhury and Mohamed [15] | $\dot{\gamma} = 9.4 \times 10^{6} \frac{D_0 G b}{kT} \left(\frac{b}{d}\right)^{2.4} \left(\frac{\tau - \tau_0}{G}\right)^{2.5} \exp\left(-\frac{76\,000}{RT}\right)$ |
| Present work | $\dot{\gamma} = 8 \times 10^{-6} \frac{D_0 G b}{kT} \left(\frac{b}{d}\right)^{2.0} \left(\frac{\tau}{G}\right)^{1.0} \exp\left(-\frac{62\,000}{RT}\right)$ |

## 3.5. Comparison of the observed flow behaviour with that reported by earlier investigators

Yavari and Langdon [1] have analysed various sets of experimental observations pertaining to Region I superplasticity in Zn–22% Al. Experimental relations compiled by Yavari and Langdon [1] and that reported by Chaudhury and Mohamed [15] are reproduced in Table IV. For the sake of comparison, the relationship obtained in the present study is included. It is evident from Table IV that though the present relationship bears some similarities to those reported earlier, it does not agree fully with any one of the earlier ones. Earlier observations (Table IV) can be classified into two types; one predicting a higher stress exponent (2.5–3.8), and the other predicting a stress exponent of unity ($\sim 1$). In the three investigations that yielded $n = 1$, the phase-size exponent ranged from $-2$ to $-3$ and the activation energy lay in the range 64.5–95.9 kJ mol$^{-1}$ [2–4]. In the three sets of experiments revealing higher value of $n$ (2.5–3.8), phase-size exponent and activation energy, respectively, varied from 2.4–2.8 and 76–119 kJ mol$^{-1}$. The dimensionless constant differed by several orders of magnitude.

There were arguments in the literature against both the types of behaviour. The data points leading to higher stress exponents were attributed to concurrent phase growth. On the other hand, the data giving rise to a stress exponent of unity were considered to be influenced by transient effects. In the present study these two effects have been duly eliminated. Fig. 3, for instance, reveals the clear onset of steady state after a transient stage. Moreover, as mentioned earlier, phase-size stability was ensured by carrying out measurements before and after the test.

Using the relationships given in Table IV, creep rates are calculated for a typical set of experimental conditions: $d = 1.98$ μm, $T = 473$ K and $\tau/G = 10^{-5}$. Calculated creep rates are given in Table V which may be compared with the present observed values for the conditions chosen. It is seen from Table V that the creep rates differ by nearly three orders of magnitude. The present study confirms a stress exponent of unity and thereby disagrees with the earlier investigations reporting a stress exponent of 2.5–3.8. However, the calculated creep rate as per the flow relationship reported by Chaudhury and Mohamed [15] matches well the creep rate derived from the present study. On the other hand, creep rates reported by other investigators (with $n \sim 1.0$) are two to three orders of magnitude faster than those observed in the present study. Besides higher creep rates, there are discrepancies with respect to phase-size exponent and activation energy. It is difficult to explain these discrepancies in the absence of complete information pertaining to experimentation and the material of the earlier workers but the higher sensitivity of the present test technique is worth reiterating in this context.

TABLE V Creep rates derived from various phenomenological equations given in Table IV for selected conditions of $\tau/G = 10^{-5}$, $T = 473$ K and $d = 1.98$ μm

| Reference | $\dot{\gamma}$ ($s^{-1}$) |
|---|---|
| Vaidya *et al.* [2] | $1.5 \times 10^{-6}$ |
| Misro and Mukherjee [4] | $4.7 \times 10^{-5}$ |
| Arieli *et al.* [3] | $6.7 \times 10^{-6}$ |
| Langdon and co-workers [7, 8] | $1.3 \times 10^{-7}$ |
| Vale *et al.* [13] | $3.7 \times 10^{-7}$ |
| Chaudhury and Mohamed [15] | |
| Grade 1 (180 p.p.m. impurities) | $1.86 \times 10^{-8}$ |
| Grade 3 (6 p.p.m. impurities) | $9.36 \times 10^{-7}$ |
| Equation 2 of present work | $5.0 \times 10^{-8}$ |
| Present experimental value | $4.7 \times 10^{-8}$ |

## 3.6. Comparison of measured creep rates with the predictions of classical Coble diffusion creep theory

Measured creep rates are compared in Table VI with

TABLE VI A comparison between measured and theoretical creep rates

| Test no. | $d$ (μm) | $T$ (K) | Measured $d\dot{\varepsilon}/d\sigma$ ($10^{-9}\,m^2(MN)^{-1}s^{-1}$) | Calculated Coble creep rate, $(d\dot{\varepsilon}/d\sigma)_{Co}$ ($10^{-5}m^2(MN)^{-1}s^{-1}$) | Measured/(calculated)$_{Co}$, $d\dot{\varepsilon}/d\sigma$ ($\times 10^4$) |
|---|---|---|---|---|---|
| SP-1 | 0.87 | 393 | 10.2 | 4.4 | 2.3 |
| SP-2 | 0.87 | 413 | 26.7 | 10.8 | 2.5 |
| SP-3 | 0.87 | 433 | 53.1 | 24.7 | 2.2 |
| SP-4 | 0.87 | 453 | 202.5 | 52.0 | 3.9 |
| SP-5 | 1.48 | 413 | 8.4 | 2.2 | 3.8 |
| SP-6 | 1.48 | 433 | 15.7 | 5.0 | 3.2 |
| SP-7 | 1.48 | 453 | 29.7 | 10.6 | 2.8 |
| SP-8 | 1.48 | 473 | 74.3 | 20.9 | 3.6 |
| SP-9 | 1.98 | 433 | 11.4 | 2.1 | 5.5 |
| SP-10 | 1.98 | 450 | 15.9 | 4.4 | 3.6 |
| SP-11 | 1.98 | 473 | 45.0 | 8.7 | 5.2 |

those predicted by the Coble theory, namely

$$\frac{d\dot{\varepsilon}}{d\sigma} = \frac{150}{\pi}\frac{w\Omega}{d^3 kT} D_{0_B}\exp\left(-\frac{Q_B}{RT}\right) \qquad (3)$$

where $w$ is the effective grain-boundary width, $\Omega$ the atomic volume and $Q_B$ the activation energy for boundary diffusion. A marked discrepancy is seen between the theory and the experiment. Measured creep rates are more than three orders of magnitude slower than those predicted by the Coble theory. The observed discrepancy between theory and experiment cannot be explained on the basis of a threshold stress [26] because the experiments revealed the absence of threshold stress.

The Coble creep process describes the flow arising out of transport of matter in a single-phase microstructure, and the procedure to extend the theory to a microduplex alloy is not clear. For a microduplex alloy such as Zn–22% Al, one can assume a constant strain model [27] wherein each phase deforms at the same strain rate as the overall strain rate, i.e. $\dot{\varepsilon}_\alpha = \dot{\varepsilon}_\beta = \dot{\varepsilon}_{\alpha+\beta}$, where $\alpha$ is the aluminium-rich phase and $\beta$, the zinc-rich phase. If the flow of each phase were to follow the Coble creep equation, the predicted creep behaviour does not match that experimentally observed. Consider a set of experimental conditions: phase size of 1.98 μm, test temperatures of 473 K and a strain rate of $10^{-8}\,s^{-1}$. The stress required to impose a strain rate of $10^{-8}\,s^{-1}$ in each phase is found to be $\sigma_\alpha = 3.6\times10^{-4}\,MN\,m^{-2}$ and $\sigma_\beta = 4\times10^{-4}\,MN\,m^{-2}$. This yields an overall calculated stress of $\sigma_{\alpha+\beta} = 3.8\times10^{-4}\,MN\,m^{-2}$ which is obtained using the expression

$$\sigma_{\alpha+\beta} = x_\alpha\sigma_\alpha + x_\beta\sigma_\beta$$

where $x_\alpha$ and $x_\beta$ are volume fractions of $\alpha$ and $\beta$ phases, respectively. This is much lower than the stress of $0.22\,MN\,m^{-2}$ obtained experimentally. Therefore, a straight-forward distribution of stresses amongst the two phases does not explain the observed results.

Chen [28] has developed a theory of diffusion creep in two-phase binary alloys. In the absence of long-range connectivity of either phase, he has shown that diffusion creep is controlled by the fastest diffusing species along its fastest path and is necessarily accompanied by migration of the phase boundaries. In developing this theory the contribution of short-circuit diffusion along interfaces to the total strain has been assumed to be negligible. This assumption clearly needs to be altered if this theory has to be extended to the present case where the activation energy suggests a boundary or interface diffusion-controlled mechanism for deformation. The interface-controlled Coble creep mechanism proposed by Schneibel and Hazzledine [29] to explain the inhibition of Coble creep in Sn–Pb alloys is not directly applicable here, because it predicts a stress exponent of 2 as against unity observed in the present study. According to this mechanism, Coble creep is rate-limited not by the difusion of vacancies but by the rate of emission and absorption at the curved dislocations in the grain boundaries which are the ultimate sources and sinks of vacancies. However, the model does not consider explicitly the nature and role of interfaces in a microduplex alloy. At the present time it seems difficult to quantify the role of such interfaces for reasons outlined below.

In a microduplex alloy of the type presently investigated, there are three types of interface: interphase $\alpha/\beta$ and intergrain $\alpha/\alpha$ and $\beta/\beta$. Quantitative metallographic examination has revealed the volume fraction of the three types of interface, namely $\alpha/\alpha$, $\alpha/\beta$ and $\beta/\beta$, expressed in per cent, to be nearly 20%, 60% and 20%, respectively. The majority of the interfaces are of the $\alpha/\beta$ type which are not considered in the flow equation. The action of these boundaries as sinks and sources for vacancies is not fully understood. Further, phase connectivity, which can play an important role in deformation, has been ignored in the theory underlying the Coble equation. Experimental evidence in terms of grain-boundary sliding, an accommodation process during diffusion creep, is available in literature [10, 30, 31] which reveals that the three types of interface in microduplex superplastic alloys show very significant differences in the sliding behaviour. In Zn–22% Al, tested in Region I, large sliding offsets have been observed [10] on $\beta/\beta$ intercrystalline boundaries as well as $\alpha/\beta$ interphase boundaries. On the other hand, the offsets were reported to be minimum on $\alpha/\alpha$ boundaries. This emphasizes the need to take into account the nature of the three types of

interface while extending the classical Coble theory to microduplex alloys.

Murthy [32] confirmed the presence of Region I in Zn–Al eutectoid alloy in the absence of concurrent phase growth. It was concluded that the phase size alone as a microstructural variable is inadequate for structure–property correlations in Regions I and II. Murthy conjectured that the structure of the phase boundary between the zinc- and aluminium-rich phases, in terms of the degree of smoothness and the interfacial dislocation density, might affect the sliding process. The initially straight phase boundaries, characteristic of annealed microstructure, were found through optical metallography to become more curved with increasing amount of prestrain. In view of these findings, electron microscopy of the interfaces was undertaken in the present investigation.

A specimen subjected to the prior thermal treatment of soaking at 633 K for 17 h in an argon atmosphere followed by water quenching and subsequent ageing at 523 K for 6 h was examined under an electron microscope to analyse carefully the interphase structure. It is important to point out that scanning and optical metallography entirely fail to reveal the complexity of structure in an apparently simple microduplex alloy. Following Murthy's suggestion [32] that interphase dislocation structure may play a role in sliding, a careful examination was carried out under a variety of two-beam conditions at high magnifications ( $> 100\,000$) to detect any evidence of low-energy dislocation configurations at these boundaries. None were detected, and an example of the essentially highly disordered, dislocation-free nature of the boundaries is shown in Fig. 9 for a portion of an $\alpha/\beta$ boundary.

The surprise, however, is in regard to the observation of precipitates at interfaces. Fig. 10 reveals precipitates along the boundary between aluminium-rich grains. A distinct precipitate-free zone appears adjacent to the grain-boundary precipitates, indicating precipitation to have occurred during ageing at 523 K. X-ray spectra of the precipitate, the precipitate-free zone and the grain interior are presented in Figs 11–13. It is evident that the precipitate has the highest zinc content and the precipitate-free zone the least, besides a strong aluminium peak indicating the grains to be rich in aluminium. A mottled contrast is seen within the aluminium-rich grain (Fig. 10) suggesting that these grains have decomposed to form very fine precipitates. The grain-boundary precipitates are seen to grow along the boundary. The zinc-rich grains (Fig. 14) contain a fine distribution of precipitates as well, whose nature has not been analysed. The TEM study thus reveals that the microstructure is complex, with precipitates along phase boundaries as well as within the phases. The presence of precipitates on $\alpha/\alpha$ boundaries explains the earlier observation [10] that sliding offsets were smallest on these boundaries.

The influence of precipitate-denuded zone on diffusional creep is not yet understood. On the other hand, it is well established that the presence of particles

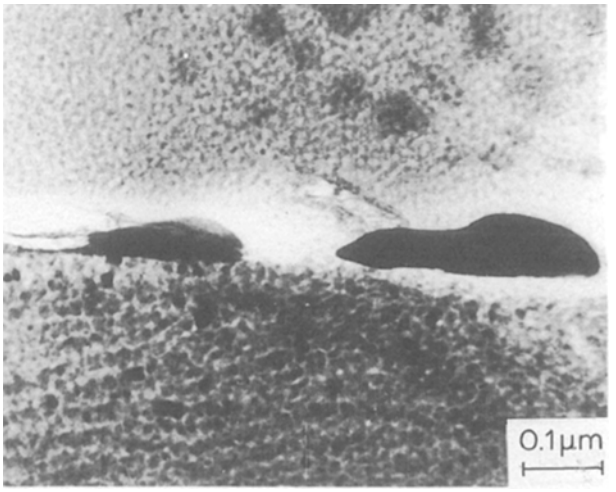


*Figure 10* Transmission electron micrograph revealing precipitates along the boundary between aluminium-rich grains after ageing at 523 K. A distinct precipitate-free zone appears adjacent to the grain-boundary precipitate.

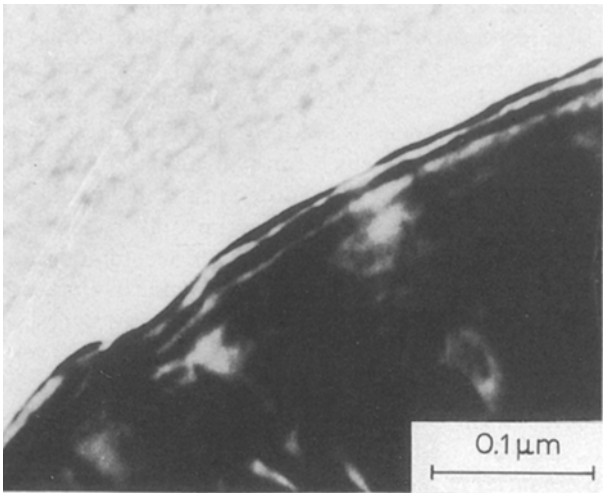


*Figure 9* A high-magnification transmission electron micrograph of the interface between the aluminium-rich and the zinc-rich grain which is seen to be free of dislocation activity.

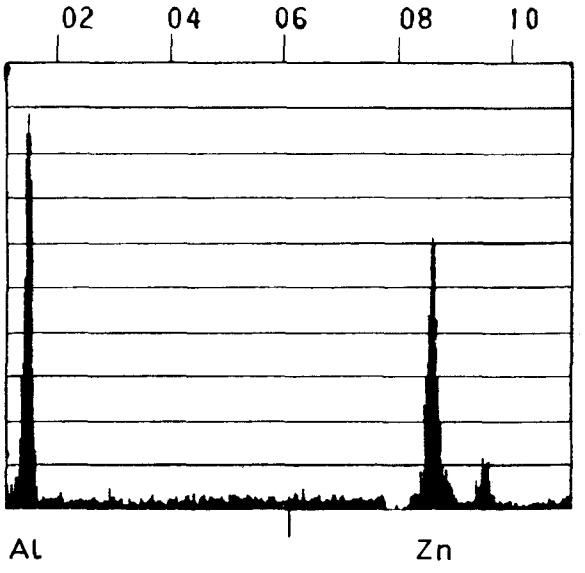


*Figure 11* X-ray spectrum of the precipitate at the Al–Al grain boundary.

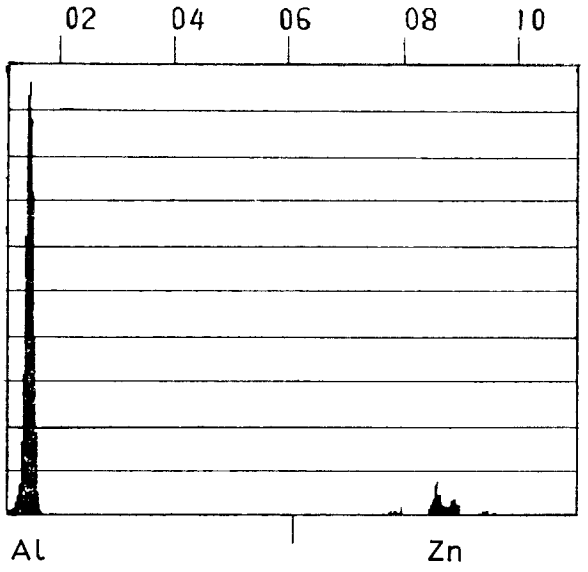


*Figure 12* X-ray spectrum of the precipitate free zone adjacent to the precipitate at the Al–Al grain boundary.

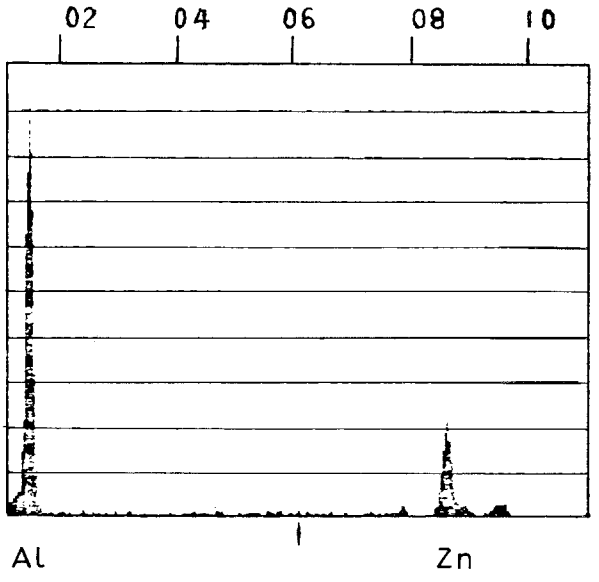


*Figure 13* X-ray spectrum of grain interior (aluminium-rich grain).

within the matrix [33] as well as at the grain/phase boundaries [34–36] can inhibit diffusional creep considerably. Decreased creep rates as compared to Coble predictions can, therefore be partly attributed to the presence of particles at α/α grain boundaries and within α and β phases. (However, no threshold stress has been observed in the present study, as predicted by the various models [37].)

## 4. Conclusions

Low-stress creep behaviour of microduplex Zn–22% Al superplastic alloy was studied in the phase-size range 0.87–1.98 μm, temperature interval 393–473 K and stresses extending up to 1.0 MN m$^{-2}$. The following conclusions emerge.

1. Steady-state creep rate varies linearly with applied stress at stresses below the transition stress, suggesting a viscous creep mechanism. Extrapolation of strain rate versus stress plot to zero strain rate revealed negligible threshold stress.

2. At stresses above the transition stress, a stress exponent of nearly 2 characteristic of Region II superplasticity has been observed.

3. Measured creep rates in Region I superplasticity can be represented by the flow relationship

$$\dot{\gamma} = 8 \times 10^{-6} \frac{D_{0_B} G \boldsymbol{b}}{kT} \left(\frac{\boldsymbol{b}}{d}\right)^2 \left(\frac{\tau}{G}\right)^{1.0} \exp\left(-\frac{62\,000}{RT}\right)$$

4. The creep activation energy of 62 kJ mol$^{-1}$ matches well that for boundary self diffusion in zinc.

5. The temperature and stress dependence of creep rate points to the occurrence of Coble creep. However, the measured phase-size exponent ($-2$) deviates from the Coble-creep predicted value of $-3$. Further, Coble-theory predicted rates are three to four orders of magnitude faster than those measured experimentally.

6. Transmission electron microscopy revealed discrete precipitation (accompanied by precipitate denuded zone) along α/α grain boundaries. Fine precipitates were also seen within the α and β phases. The lower values of the measured creep rates as compared to the Coble-theoretical rates can be partly understood in terms of the inhibiting action of these precipitates on the diffusional flow. Although the comprehensive role played by the three different types of interface, namely α/α, α/β and β/β in diffusion creep is not fully understood, the present observation that the α/β interfaces were essentially highly disordered boundaries is noteworthy from the view point that this feature is unlikely to contribute to reduced creep rates.

7. There is a strong indication that microstructural features discussed in the foregoing can be responsible for discrepancies between the experimentally observed creep behaviour and Coble theory predictions, originally developed for single-phase materials. However, a quantitative analysis of the influence of the microstructural parameters in a microduplex alloy calls for another major effort due to the complexities indicated.

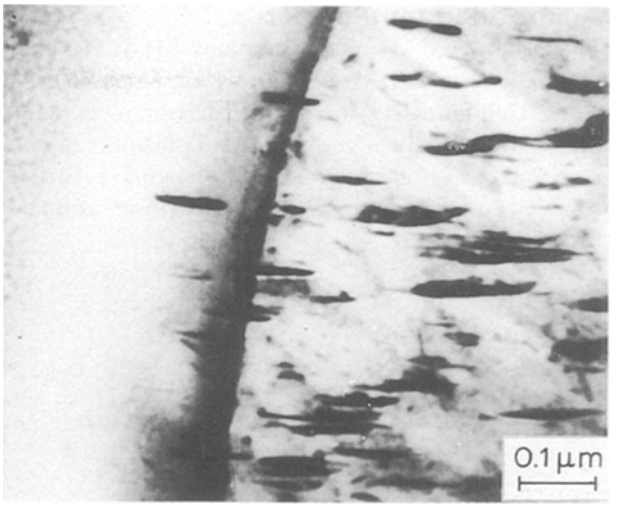


*Figure 14* Transmission electron micrograph revealing fine distribution of precipitates in the zinc-rich grains.

## Acknowledgements

The authors (G. M. and D. B.) thank Mr SLN Acharyulu, Director, DMRL for permission to publish this work. Helpful discussion with Professor A. K. Mukherjee is gratefully acknowledged. Transmission electron microscopy carried out by Professor J. L. Strudel revealed equiaxed grain structure; this observation has been included here.

## References

1. P. YAVARI and T. G. LANGDON, *Mater. Sci. Engng* **57** (1983) 55.
2. M. L. VAIDYA, K. L. MURTHY and J. E. DORN, *Acta Metall.* **21** (1973) 1615.
3. A. ARIELI, A. K. S. YU and A. K. MUKHERJEE, *Metall. Trans.* **11A** (1980) 181.
4. S. C. MISRA and A. K. MUKHERJEE, in "Rate Processes in Plastic Deformation of Materials", edited by J. C. M. Li and A. K. Mukherjee (ASM, Metals Park, OH, 1975) p. 434.
5. R. S. MISHRA and G. S. MURTY, *J. Mater. Sci.* **23** (1988) 593.
6. H. ISHIKAWA, F. A. MOHAMED and T. G. LANGDON, *Phil. Mag.* **32** (1975) 1269.
7. F . A. MOHAMED and T. G. LANGDON, *Acta Metall.* **23** (1975) 117.
8. F. A. MOHAMED, S. A. SHEI and T. G. LANGDON, *ibid.* **23** (1975) 1443.
9. F. A. MOHAMED, M. M. I. AHMED and T. G. LANGDON, *Metall. Trans.* **8A** (1977) 933.
10. P. SHARIAT, R. B. VASTAVA and T. G. LANGDON, *Acta Metall.* **30** (1982) 285.
11. D. GRIVAS, J. W. MORRIS and T. G. LANGDON, *Scripta Metall.* **15** (1981) 229.
12. D. GRIVAS, Rep. LBL-7375, Lawrence Berkeley Laboratory, University of California, Berkeley, CA (1978).
13. S. H. VALE, D. J. EASTGATE and P. M. HAZZLEDINE, *Scripta Metall.* **13** (1979) 1157.
14. D. W. LIVESEY and N. RIDLEY, *ibid.* **16** (1982) 165.
15. P. K. CHAUDHURY and F. A. MOHAMED, *Acta Metall.* **36** (1988) 1099.
16. D. J. TOWLE and H. JONES, *ibid.* **24** (1976) 399.
17. G. MALAKONDAIAH and P. RAMA RAO, *Trans. Ind. Inst. Metals* **31** (1978) 361.
18. W. ROSTOKER and J. R. DVORAK, "Interpretation of Metallographic Structures", 2nd Edn (Academic Press, New York, 1977).
19. E. S. WAJDA, *Acta Metall.* **2** (1954) 184.
20. T. S. LUNDY and J. F. MURDOCK, *J. Appl. Phys.* **33** (1962) 671.
21. G. A. SHIRN, E. S. WAJDA and H. B. HUNTINGTON, *Acta Metall.* **1** (1953) 513.
22. K. A. PADMANABHAN and G. J. DAVIES, in "Superplasticity" (Springer, Berlin, Heidelberg, 1980).
23. F. R. N. NABARRO, "Reports of the Conference on the Strength of Solids" (Physical Society, London, 1948) p. 75.
24. C. HERRING, *J. Appl. Phys.* **21** (1950) 437.
25. R. L. COBLE, *ibid.* **34** (1963) 1679.
26. M. F. ASHBY and R. A. VERRALL, *Acta Metall.* **21** (1973) 149.
27. J. J. KEARNS, J. E. McCAULEY and F. A. NICHOLS, *J. Nucl. Mater.* **61** (1976) 169.
28. L. W. CHEN, *Acta Metall.* **30** (1982) 1655.
29. J. H. SCHNEIBEL and P. M. HAZZLEDINE, *J. Mater. Sci.* **18** (1983) 562.
30. R. B. VASTAVA and T. G. LANGDON, *Acta Metall.* **27** (1979) 251.
31. T. CHANDRA, J. J. JONAS and D.M.R. TAPLIN, *J. Mater. Sci.* **13** (1978) 2380.
32. G. S. MURTHY, *Scripta Metall.* **20** (1986) 533.
33. K. E. EASTERLING and G. H. GESSINGER, *Z. Metallkde* **63** (1972) 237.
34. M. F. ASHBY, *Scripta Metall.* **3** (1969) 837.
35. B. BURTON, *Mater. Sci. Engng* **11** (1973) 337.
36. J. E. HARRIS, *Metal Sci. J.* **7** (1973) 1.
37. B. BURTON, "Diffusional Creep of Polycrystalline Materials" (Trans. Tech. Publications, Aedermannsdorf, Switzerland, 1977).

*Received 12 November 1991*
*and accepted 14 August 1992*